Biomaterials Science

ROYAL SOCIETY OF CHEMISTRY

PAPER

View Article Online
View Journal | View Issue

Cite this: *Biomater. Sci.*, 2026, **14**, 2027

Nanocellulose with dual carboxy and aldehyde functionality: a modular platform for hydrogel formation and sustained drug release

Emanuela Bua, †[a] Chiara Spanu, †[a] Giovanni Inzalaco, [b] Martina Zangari, [a] Luca Sartorelli, [a] Letizia Sambri, [a] Elisabetta Venuti, [a] Tommaso Salzillo, [a] Mauro Comes Franchini, [a] Mario Chiariello[c,d] and Erica Locatelli *[a]

Nanocellulose-based hydrogels hold great promise for biomedical applications, particularly as localized drug delivery systems, due to their biocompatibility, tunable porosity, and soft-tissue mimicking properties. However, most reported systems rely on single-mode crosslinking strategies and exhibit rapid burst release, limiting sustained therapeutic delivery. Herein, we report the synthesis and full characterization of a novel bifunctional crystalline nanocellulose bearing both carboxy and dialdehyde groups. This dual-functionalization was achieved *via* a sequential (2,2,6,6-tetramethylpiperidin-1-yl)oxidanyl (TEMPO)-mediated oxidation followed by sodium periodate treatment, enabling reactivity with diamine-based crosslinkers. Hydrogels were prepared using either spermine or ε-poly-L-lysine through electrostatic or covalent crosslinking. The resulting materials exhibited tunable rheological properties, homogeneous and porous structures, and high *in vitro* biocompatibility. As a proof-of-concept, the chemotherapeutic agent doxorubicin was incorporated into selected hydrogel formulations, showing a sustained release over three weeks without a burst effect. These findings highlight the potential of bifunctional CNCs as a modular and customizable platform for the development of injectable hydrogels for prolonged local drug delivery.

Received 16th December 2025,
Accepted 23rd February 2026

DOI: 10.1039/d5bm01841b

rsc.li/biomaterials-science

1. Introduction

Nanocellulose, in its crystalline (CNCs) or fibrillated (CNFs) form, is widely recognized for its biocompatibility, reinforcing properties and modifiable surface chemistry, making it an ideal platform for advanced biomaterials.[1] Among its many modifications, surface oxidation remains a key strategy to introduce functional groups that enable further derivatization or crosslinking. Traditionally, TEMPO ((2,2,6,6-tetramethylpiperidin-1-yl)oxidanyl)-mediated oxidation selectively converts primary hydroxy groups at C6 into carboxylic acids,[2] while periodate oxidation cleaves the C2–C3 vicinal diols,[3] generating aldehyde functionalities. However, to date, the coexistence of both functional groups (carboxylic acid at C6 and aldehydes at C2 and C3) on the same nanocellulose scaffold has remained elusive or insufficiently explored, largely due to cross-reactivity and instability of aldehydes under standard multi-step oxidation conditions. Notably, Mendoza *et al.*[4] reported a one-pot approach combining TEMPO and periodate oxidation to obtain highly functionalized cellulose nanofibers, but aldehyde groups were largely consumed or converted into carboxylic acids under the reaction conditions, limiting their availability and orthogonal reactivity. Similarly, Patterson and Hsieh[5] developed a sequential periodate–chlorite oxidation to tune the balance between dialdehyde and dicarboxylate nanocelluloses at the C2 and C3 positions; however, this strategy did not incorporate C6-selective carboxylation, and aldehyde functionality remained transient and difficult to preserve.

To the best of our knowledge, no prior work has demonstrated the stable and simultaneous presence of carboxy and dialdehyde groups on CNCs with preserved structural integrity. This dual functionalization not only may expand the chemical versatility of the CNC surface, but also significantly enhances the potential for cross-linking strategies. Indeed, the simultaneous presence of carboxy and aldehyde groups enables crosslinking *via* complementary mechanisms, such as ionic interactions with amines and/or covalent imine (Schiff base) or

[a]*Department of Industrial Chemistry "Toso Montanari", Via Gobetti 85, 40129 Bologna, Italy. E-mail: erica.locatelli2@unibo.it*
[b]*Institute of Endotypes in Oncology, Metabolism and Immunology "Gaetano Salvatore", National Research Council, Via Pansini 5, 80131 Napoli, Italy*
[c]*Core Research Laboratory (CRL), Istituto per lo Studio la Prevenzione e la Rete Oncologica (ISPRO), Via Fiorentina 1, 53100 Siena, Italy*
[d]*Institute of Clinical Physiology, National Research Council, Via Fiorentina 1, 53100 Siena, Italy*
† These authors contributed equally to this work.

amide linkages, offering a versatile platform for the development of advanced materials such as hydrogels. Beyond increasing surface reactivity, the simultaneous presence of carboxyl and aldehyde groups on the same nanocellulose scaffold provides a chemical basis for the formation of hydrogel networks relying on complementary crosslinking mechanisms. Covalent amide bonds generated *via* carbodiimide chemistry yield stable and long-lived connections, while ionic interactions and reversible imine (Schiff base) linkages introduce weaker and more labile interactions.

Hydrogels derived from nanocellulose have attracted increasing attention in the field of biomedical engineering due to their high-water content, soft-tissue mimicking properties, biocompatibility, and mechanical tunability.[6] Their ability to form interconnected porous networks makes them excellent candidates for drug delivery platforms, localized cancer therapy, tissue engineering scaffolds, and wound dressings. In particular, in drug delivery of locally administered therapeutics, nanocellulose hydrogels may allow for sustained and prolonged drug release over time; the possibility of having a drug release that lasts days or weeks is a critical aspect to maximize therapeutic efficacy while minimizing systemic toxicity and, equally, avoiding burst release is crucial in local therapeutics, as an initial drug surge may exceed the therapeutic window, causing tissue irritation and leading to premature drug depletion, thus compromising sustained efficacy.[7] Unfortunately, most of the existing nanocellulose-based hydrogels, which rely on single-mode cross-linking mechanisms, often exhibit burst-release behaviour, releasing most of their drug payload within a few hours or, at best, a couple of days. For instance, the most promising CNC-based hydrogels crosslinked with chitosan or gelatin have shown rapid release profiles, with up to ~70% of the loaded drug released within 4 hours and nearly complete release occurring in less than 24 hours.[8,9]

A bifunctional nanocellulose scaffold, offering complementary and site-selective reactivity, may thus provide a more robust and customizable platform for the design of next-generation hydrogel systems for biomedical use.

Herein, we report the successful synthesis and full characterization of a novel bifunctional crystalline nanocellulose bearing simultaneously carboxy and dialdehyde groups, achieved *via* a controlled sequential oxidation strategy combining TEMPO and sodium periodate chemistries. Exploiting this bifunctionality, we developed nanocellulose-based hydrogels using biocompatible diamines, such as spermine and poly-L-lysine, as crosslinking agents. The hydrogels were formed either physically, by ionic and imine interactions, or chemically, by common carbodiimide-mediated coupling. The resulting materials exhibited promising rheological properties, optimal porosity, high *in vitro* biocompatibility and capacity to incorporate hydrophilic drugs. As a proof-of-concept, we encapsulated the chemotherapeutic agent doxorubicin within the hydrogel matrix, observing a sustained release profile over several weeks, suggesting potential applications in localized post-surgical drug delivery.

Rather than defining a single optimal formulation, this hybrid bonding landscape enables a modular tuning of network properties, allowing mechanical behaviour, stability, and release profiles to be adjusted by selecting the type of crosslinking and crosslinker employed. In this context, dual-functional nanocellulose represents a versatile platform for designing hydrogels with tailored properties, without relying exclusively on a single-mode crosslinking strategy.

2. Results and discussion

2.1. Synthesis and characterization of modified nanocellulose

2.1.1. Synthesis of modified nanocellulose. Following an already established procedure,[10] nanocellulose was obtained by means of sulfuric acid hydrolysis of cellulose filter paper. In this way, acid hydrolysed the amorphous regions of cellulose, leaving the crystalline ones untouched, thus generating cellulose nanocrystals (CNCs), which can be easily purified by centrifugation and washing with water. The purified CNC suspension was subsequently involved in the first oxidation step, indicating the TEMPO-oxidation reaction. This was performed using the TEMPO/NaBr/NaClO combination, leading to the formation of carboxylic acid groups at the C6 positions of the cellulose backbone. TEMPO-oxidation involves the use of TEMPO as a catalyst and NaClO as an oxidant to selectively oxidise the carbon bearing a primary alcohol into an aldehydic moiety, which under the alkaline conditions (pH 10) of the reaction environment immediately leads to carboxylic acid groups.[11] To achieve the desired dual functionality, the carboxy groups must be introduced first, followed by the aldehyde groups. This order is essential because aldehydes would otherwise be further oxidized under the TEMPO conditions. Indeed, the so-obtained carboxylated nanocellulose (CNCs–COOH) was at first purified through dialysis and then further oxidised to introduce aldehyde groups onto the surface, by using sodium periodate ($NaIO_4$). Periodate oxidation implies the cleavage of the C–C bond between carbons 2 and 3 of the glucose monomers of CNCs,[3] resulting in the ring opening and formation of aldehydic groups, without affecting the carboxylic acid already present in the structure. The reaction should be controlled strictly to convert only the surface of the cellulose nanocrystals and spare the core of the materials, so as to not affect their final properties. The reaction procedure adopted for the double oxidized nanocellulose (CNCs–COOH–CHO) synthesis is reported in Fig. 1.

Two storage conditions were investigated: CNCs–COOH–CHO in the form of liquid suspension was stored at 4 °C for 30 days, while the freeze-dried product was stored at rt for 6 months. In Fig. S1, the stability of the aldehyde group is assessed through ATR-FTIR spectroscopy. This qualitative analysis demonstrates only a slight decrease in the intensity of the aldehyde peaks after 30 days and 6 months of observation, which is consistent with the expected gradual degradation of the aldehyde functionality over time.

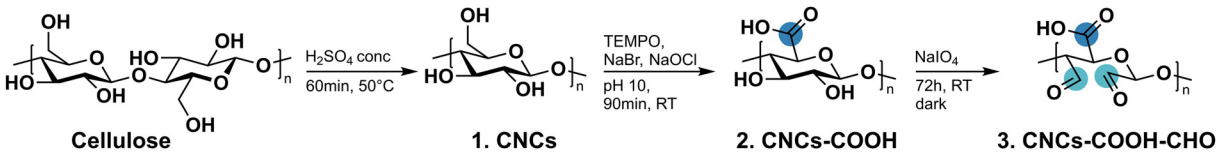

Fig. 1 Synthetic approach to achieve nanocellulose and its oxidised forms.

2.1.2. ATR-FTIR characterization. ATR-FTIR spectroscopy was used to characterize the oxidized nanocellulose derivatives. Fig. 2 compares pristine CNCs with the two oxidized products, carboxylated nanocellulose (CNCs–COOH) and carboxylated nanocellulose bearing aldehyde groups (CNCs–COOH–CHO). The spectra retain the characteristic vibrational features of cellulose with no significant shifts, indicating that the oxidation steps do not alter the CNC backbone and that the reaction conditions are sufficiently mild. A detailed assignment of the main cellulose bands is provided in the SI (Table S1). As highlighted in the inset of Fig. 2, TEMPO-mediated oxidation is evidenced by the appearance of the carboxyl C═O stretching band at 1721 cm^{-1} in CNCs–COOH. In addition, the relative intensity of the 2900–3335 cm^{-1} region decreases after oxidation, in agreement with a partial consumption of the C–H/O–H groups during functionalization; consistently, a shoulder around ~1600 cm^{-1} can be attributed to carboxylate ($–COO^-$/–COONa) groups. In CNCs–COOH–CHO, subsequent $NaIO_4$ oxidation is confirmed by the emergence of a new band at 1733 cm^{-1}, assigned to aldehyde C═O stretching.

2.1.3. DLS analyses. Dynamic Light Scattering (DLS) analysis was performed to evaluate surface charge density through zeta potential (Potζ) measurement. The zeta potentials of different batches were determined from 15–25 individual measurements, with the DLS system averaging the results of each run to provide a final value. Within the average zeta potential, mean standard deviations were calculated as the square root of the average variance (see the SI, Table S2). Pristine CNCs exhibited a negative surface charge of −27.9 ± 4.71 mV, which is commonly attributed to the presence of anionic groups introduced during sulfuric-acid hydrolysis. A more negative ζ-potential (−4 2.5 ± 3.71 mV) was observed for CNCs–COOH, consistent with the formation of carboxylic acid groups that are deprotonated at physiological pH, further confirming the success of TEMPO-mediated oxidation. After periodate oxidation, CNCs–COOH–CHO exhibited a slightly less negative ζ-potential (−34.6 ± 4.07 mV). Since aldehyde groups are neutral and cellulose hydroxyl groups are essentially non-ionized at pH ≈ 6.5, this variation is not attributed to a direct change in surface charge associated with –CHO formation. Rather, under low-ionic-strength conditions, such differences may reflect changes in interfacial properties and/or the counterion environment following the additional oxidation and purification steps.

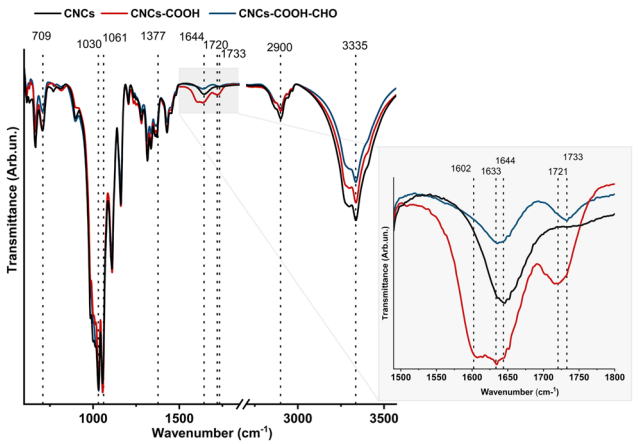

Fig. 2 ATR-FTIR comparison between the spectra of CNCs (black line) and both oxidised nanocellulose products (CNCs–COOH, red line and CNCs–COOH–CHO, blue line). The grey boxed area highlights the zoomed-in region between 1500 and 1800 cm^{-1}.

2.1.4. Carboxy and aldehyde group quantification. TEMPO-oxidation of nanocellulose (CNCs) to carboxylated nanocellulose (CNCs–COOH) was optimized in terms of reaction time and the moles of oxidative agent used (see the SI, Table S3). At the end of the reactions, in order to quantify the degree of oxidation of the CNCs–COOH, and thus the amount of carboxylic acids present, conductometric titrations were performed. Specifically, an aqueous suspension of modified CNCs at a concentration of 14.6 mg mL^{-1} was prepared and subsequently acidified with a 0.100 M HCl solution to a pH of ≃3.00. The conductometric titration was carried out by the gradual addition of 0.100 M NaOH. The resulting titration curve typically exhibits three distinct regions, which, proceeding from left to right, correspond to (i) the neutralization of strong acids, (ii) the neutralization of weak acids, and (iii) the presence of excess base.[12] By evaluating the volume of titrant consumed in the second region (ii), it is possible to quantify the moles of carboxylic acid groups present (see the SI, Fig. S2). The quantitative data obtained *via* conductometric titrations for the evaluation of the amount of carboxylic acids present in each sample refer to measurements performed in triplicate, after considering the null contribution from pristine CNCs (Fig. S3). In particular, the value changed from a minimum of 0.043 ± 0.002 mmol g^{-1} to a maximum of 0.36 ± 0.04 mmol g^{-1}, depending on the various reaction conditions, as depicted in Table S3.

To quantify the aldehydic groups on CNCs, the Hantzsch reaction was employed (see the SI, Fig. S4 and S5, Table S4 "Calibration line data"). In this method, acetoacetanilide (AAA) reacts with formaldehyde in the presence of ammonium

acetate to form a dihydropyridine derivative, showing an absorption maximum at 368 nm and fluorescence with excitation and emission at 370 and 470 nm, respectively. The reaction is simple, rapid, and sensitive, and proceeds efficiently at room temperature without heating, making it well-suited for CNCs. Spectrophotometric detection of the dihydropyridine derivative was performed and aldehyde concentration was determined from a calibration curve based on fluorescence intensity, yielding 0.28 mmol of aldehyde groups per gram of CNCs. This result confirms the successful oxidation of CNCs and can be regarded as highly satisfactory.[13,14]

2.2. Hydrogel formulations and characterisation studies

2.2.1. Synthesis of chemically and physically crosslinked hydrogels. After obtaining concentrated and purified mono-oxidized nanocellulose (CNCs–COOH) or bi-oxidized nanocellulose (CNCs–COOH–CHO), the formation of hydrogels was attempted, by using cross-linking agents with terminal amines as functional groups, so as to allow reactivity with both aldehydes and carboxylic acids. In order to investigate the possibility of tuning the hydrogel features by controlling the functionalization of the nanocellulose, its reactivity, and the cross-linkers' length, the combination of two cross-linkers, spermine and ε-poly-L-lysine (ε-PLL), was attempted. Similarly, two kinds of reactivities were investigated: in some cases, merely physical bonds (P), such as acid–base and ionic interactions, were formed, whereas in other cases, a covalent bond between nanocellulose and the cross-linkers was created by means of a chemical reaction (C) mediated by coupling agents such as 1-ethyl-3-(3-dimethylaminopropyl)carbodiimide (EDC) and *N*-hydroxysuccinimide (NHS). Moreover, both mono-oxidized nanocellulose and bi-oxidized nanocellulose were employed to demonstrate the importance of having more functionality on the same backbone for the final hydrogels' features. The achieved hydrogels, with the selected methodologies, are reported in Table 1, Fig. S6 (physical hydrogels P1–P4) and S7 (chemical hydrogels C1–C4), whereas a general procedure for the synthesis is reported in Fig. 3. It should be noted that in all formulations containing spermine as a crosslinker, a calcium chloride solution was added to enhance stabilization of the crosslinking degree by introducing weak ionic interactions (see the SI, Table S5 "Hydrogel composition"). In physically crosslinked hydrogels, the network is typically weaker and reversible because it is sustained by non-covalent interactions. In these systems, hydrogen bonding and electrostatic attractions are expected to be the dominant contributions. In particular, protonation/deprotonation of functional groups such as carboxylic acids and amines can generate oppositely charged species that promote strong interchain interactions and, ultimately, network formation. All hydrogels (P1–P4) passed the tilt test, showing a creamy but consistent texture, indicating the formation of self-standing materials suitable for extrusion purposes. Chemical crosslinking, instead, is based on the occurrence of a chemical reaction that generates a new covalent permanent bond; the network in this approach should be stronger and more stable over time. In all formulations (C1–C4), EDC/NHS were used to activate carboxy groups, keeping their concentrations low to avoid any cytotoxicity problems (under 0.24 M), and new amidic covalent groups were thus formed thanks to the crosslinkers' amino groups. The resulting hydrogels exhibit a similar appearance, with a white, creamy texture, pass the tilt test, and remain soft enough to be extruded through a needle.

To assess the practical impact of differences in the nanocellulose degree of oxidation, the gel-forming ability and rheological behaviour of materials prepared with different degrees of oxidation were evaluated. When oxidized CNCs with a lower oxidation degree (0.043 ± 0.002 mmol g^{-1}) were used, gel formation was often not achieved, and the formulations remained liquid, indicating that the number of available functional groups was insufficient to generate a stable crosslinked network. Conversely, in the case of an intermediate oxidation degree (0.09 ± 0.02 mmol g^{-1}), the gels formed, but they were creamier than intended. Based on these observations, the oxidation degree was intentionally increased to enable the formation of self-supporting, solid-like hydrogels with reproducible rheological properties. Fig. S8 shows the amplitude sweep test curve for a gel formulated starting from CNCs–COOH with a carboxylic acid content equal to 0.09 ± 0.02 mmol g^{-1}; it can be noted that, in this case, the breaking point of the gel is lower ($\varepsilon \approx 12\%$) compared to the optimized gel C3 ($\varepsilon \approx 40.5\%$) in which the carboxylic acid content was 0.36 ± 0.04 mmol g^{-1}.

Finally, the crosslinker concentration was used as an additional tuning parameter to further stabilize the network and modulate the mechanical properties of the gels. By adjusting the crosslinker content, it was possible to obtain more robust and mechanically stable networks, ensuring consistent gel behaviour despite minor batch-to-batch variations in the starting material.

2.2.2. ATR-FTIR characterization. The developed hydrogels were subjected to physicochemical characterization to compare the features of the networks formed, starting with ATR-FTIR spectroscopy, as it directly probes the chemical nature of crosslinking, providing the basis to interpret the subsequent morphology, mechanics and performance related results. To aid band assignment, the ATR-FTIR spectra of the pristine crosslinkers (spermine and ε-poly-L-lysine) are reported in the SI (Fig. S9) together with their main diagnostic bands in Table S6.[15–17] These reference spectra are then used below to interpret changes observed after hydrogel assembly.

Table 1 Classification of hydrogels

Series	Name	CNCs' modification	Crosslinker
Chemical crosslinking	C1	CNCs–COOH	Spermine
	C2	CNCs–COOH–CHO	Spermine
	C3	CNCs–COOH	ε-Poly-L-lysine
	C4	CNCs–COOH–CHO	ε-Poly-L-lysine
Physical crosslinking	P1	CNCs–COOH	Spermine
	P2	CNCs–COOH–CHO	Spermine
	P3	CNCs–COOH	ε-Poly-L-lysine
	P4	CNCs–COOH–CHO	ε-Poly-L-lysine

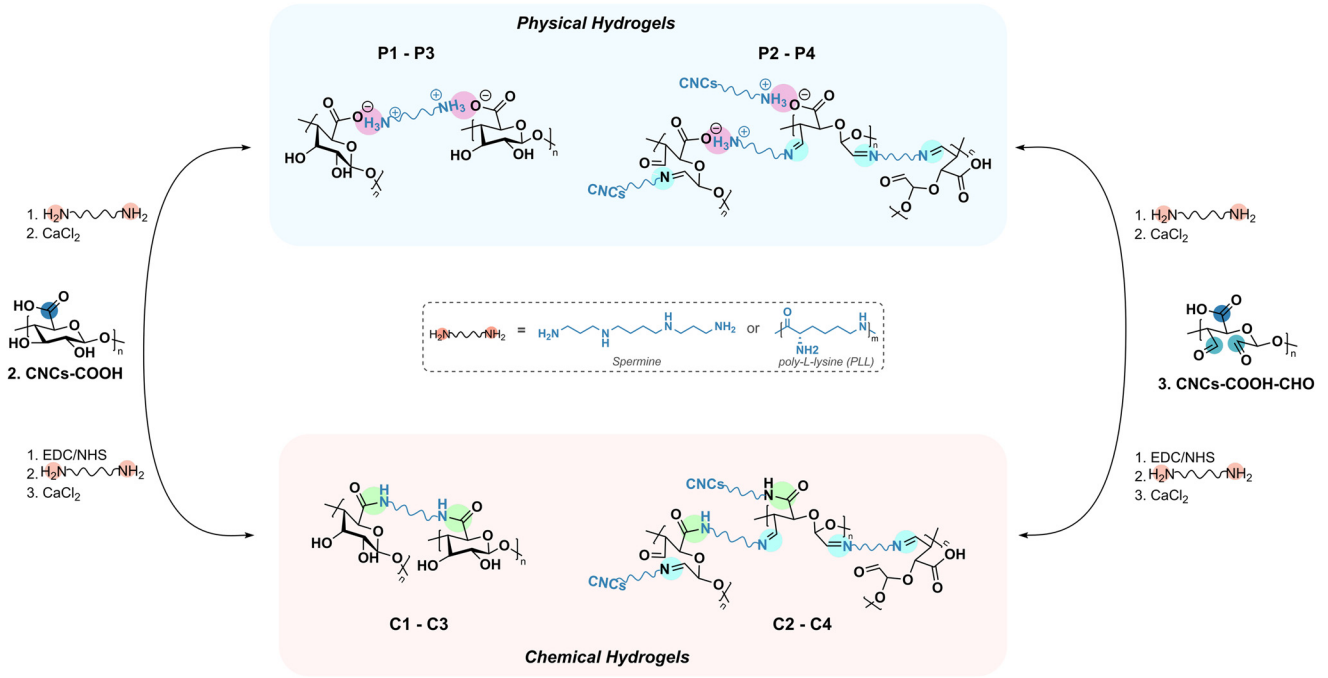

Fig. 3 Schematic representation of the proposed hydrogel formulations.

Fig. 4 shows the ATR-FTIR spectra of both physically and chemically crosslinked hydrogels. Fig. 4A and B show the ATR-FTIR spectra of physically crosslinked hydrogels of the P1–P4 series. Fig. 4A shows the spectra of P1 (CNCs–COOH + spermine) and P3 (CNCs–COOH + ε-poly-L-lysine) hydrogels, in comparison with the spectrum of CNCs–COOH. While contributions from the starting materials are still detectable (green arrows and blue arrows in the figure for spermine and ε-poly-L-lysine bands, respectively), the most diagnostic feature associated with physical gel formation is a marked red shift of the CNC carboxyl C=O stretching band down to about 1638 cm^{-1}. This shift is consistent with electrostatic interactions between carboxylate groups (COO^-) and protonated amines (NH_3^+) of spermine or ε-poly-L-lysine.[18] In addition, the broad O–H stretching envelope around 3335 cm^{-1} decreases in intensity in P1 and P3 relative to that of CNCs–COOH, indicating the involvement of hydroxyl groups in the interaction pattern. Fig. 4B compares P2 (CNCs–COOH–CHO + spermine) and P4 (CNCs–COOH–CHO + ε-poly-L-lysine) with CNCs–COOH–CHO. In both cases, network formation is accompanied by clear modifications within the 1600–1720 cm^{-1} range, where carbonyl stretching modes occur, supporting the formation of physically crosslinked networks. Additional minor bands attributable to the crosslinkers are discussed in the SI. Overall, these observed spectral changes confirm the hydrogel formation.

Fig. 4C and D show ATR-FTIR spectra of chemically crosslinked hydrogels (C1–C4). Covalent amide formation is expected to produce diagnostic absorptions in the 1500–1700 cm^{-1} region (Amide I and Amide II). In agreement with this, the inset of Fig. 4C highlights distinct bands at ~1644 cm^{-1} (Amide I) and ~1551 cm^{-1} (Amide II) for C1 (CNCs–COOH + spermine) and C3 (CNCs–COOH + ε-poly-L-lysine) compared to those of unmodified CNCs–COOH, indicating successful covalent coupling. Similarly, C2 (CNCs–COOH–CHO + spermine) and C4 (CNCs–COOH–CHO + ε-poly-L-lysine) exhibit Amide I/II features centered at 1646 and 1551 cm^{-1}, respectively (Fig. 4D), confirming amide bond formation across all chemically crosslinked systems. A complete list of peak positions and assignments for the pristine crosslinkers and for all hydrogel formulations is provided in Table S7 (see the SI).

2.2.3. Rheological measurements. Rheological properties of chemically or physically crosslinked hydrogels were measured using an Anton Paar rheometer equipped with a parallel plate geometry with DPP25 as the upper plate. Amplitude sweep tests were conducted to determine storage (G') and loss moduli (G'') providing insight into the viscoelastic behaviour and structural integrity of the gel networks under increasing shear strain.

For all investigated formulations, G' was consistently higher than G'' over the tested strain range, indicating a predominantly elastic response and confirming the solid-like behaviour of all eight hydrogels.

Although both physically (Fig. 5A and B) and chemically crosslinked hydrogels (Fig. 5C and D) exhibited comparable G'/G'' ratios within the linear viscoelastic region (LVR), clear differences emerged in terms of network stability. Chemically crosslinked hydrogels presenting mono-oxidised nanocellulose exhibited a wider and more stable LVR, maintaining constant viscoelastic moduli up to a strain of approximately $\varepsilon \approx 1.5\%$. In contrast, physically crosslinked hydrogels showed a nar-

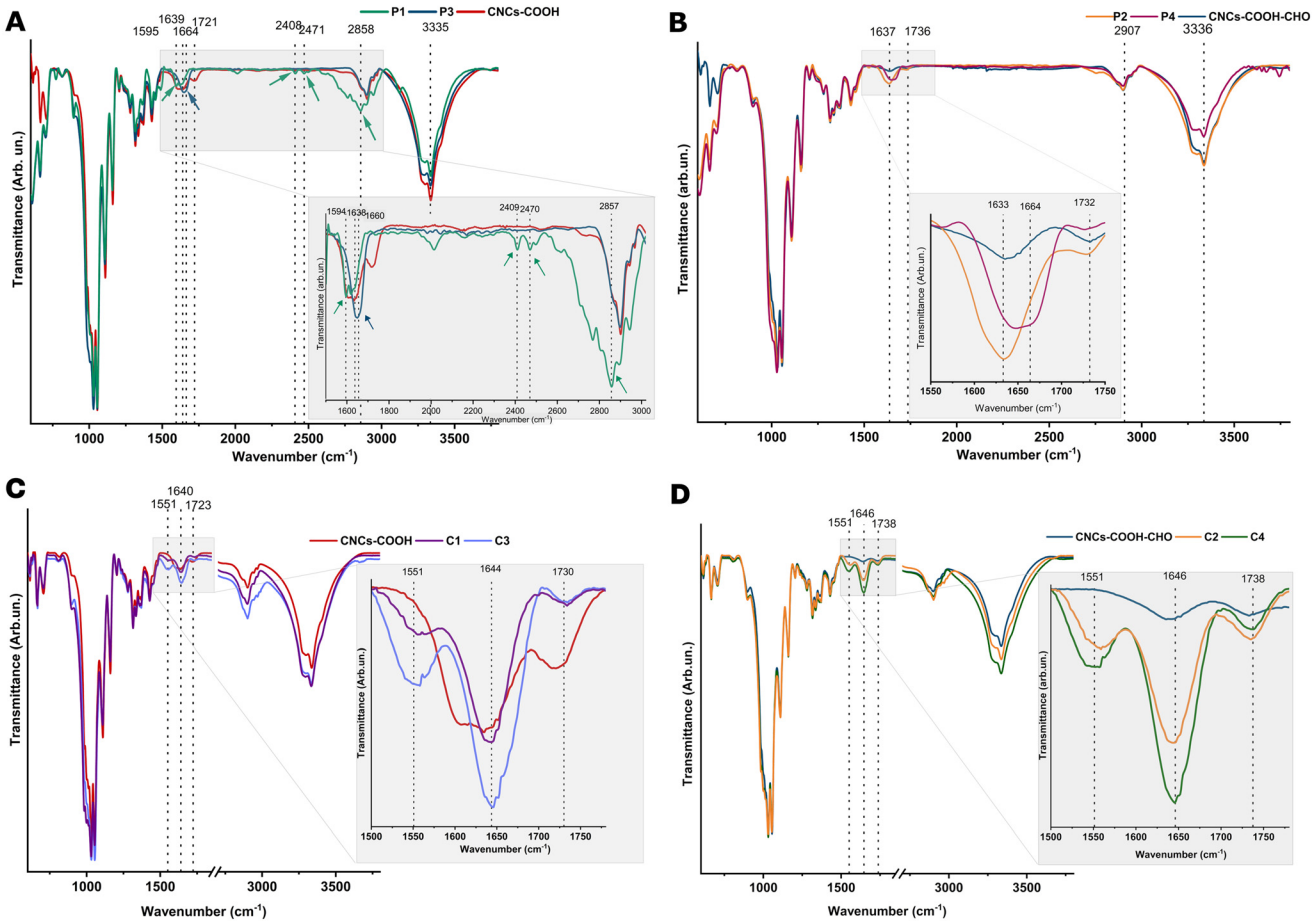

Fig. 4 ATR-FTIR spectra of the P1–P4 series (A and B) and the C1–C4 series (C and D). (A) P1 (CNCs–COOH + spermine, green line), P3 (CNCs–COOH + ε-poly-L-lysine, light blue line), and CNCs–COOH (red line). The green and light blue arrows highlight spermine and ε-poly-L-lysine in P1 and P3, respectively. (B) P2 (CNCs–COOH–CHO + spermine, orange line), P4 (CNCs–COOH–CHO + ε-poly-L-lysine, purple line), and CNCs–COOH–CHO (blue line). (C) C1 (CNCs–COOH + spermine, purple line), C3 (CNCs–COOH + ε-poly-L-lysine, light blue line), and CNCs–COOH (red line). (D) C2 (CNCs–COOH–CHO + spermine, orange line), C4 (CNCs–COOH–CHO + ε-poly-L-lysine, green line), and CNCs–COOH–CHO (blue line). The insets in panels A and B highlight the amide region.

rower LVR, limited to around 0.4% strain, followed by a more pronounced decrease in both moduli. This behaviour reflects the intrinsic differences in the network architecture: chemically crosslinked gels are stabilized by permanent covalent bonds, which confer higher resistance to deformation, whereas physically crosslinked gels rely on weaker, reversible interactions such as hydrogen bonding or electrostatic interactions, making them more susceptible to structural rearrangements under shear.

Within the group of chemically crosslinked hydrogels, differences in mechanical robustness were observed depending on the crosslinking agent employed. Hydrogel C3, containing ε-PLL as a crosslinker, exhibited a gel–sol transition at higher strain values ($\varepsilon \approx 41\%$) compared to hydrogel C1, *i.e.* the hydrogel with spermine as a crosslinker, which showed a crossover point at approximately 28% strain. These findings suggest a higher crosslinking efficiency or more homogeneous network formation in C3, resulting in enhanced resistance to mechanical disruption.

Conversely, among physically crosslinked hydrogels, the formulation containing spermine as a crosslinker (P1) demonstrated a higher breaking point ($\varepsilon \approx 47\%$) compared to the hydrogel synthesized using ε-PLL (P3), which exhibited a crossover at $\varepsilon \approx 32\%$. This difference can be attributed to variations in the nature and density of physical interactions governing network cohesion.

Notably, hydrogels based on CNCs–COOH–CHO exhibited a shorter LVR and an earlier onset of structural failure compared to CNCs–COOH-based gels. The presence of both carboxylic acid and dialdehyde functionalities, resulting from double oxidation of nanocellulose, led to a denser and stiffer network. While this increased rigidity was associated with a lower breaking strain, it also indicated a more solid, tougher structure with reduced deformability. In fact, the G' and G'' moduli of these gels were an order of magnitude higher (for instance, G' was $\sim 3 \times 10^3$ Pa in P3, whereas it was $\sim 3 \times 10^4$ Pa in P4) than those of gels formed from mono-oxidised nanocellulose, making them more similar to a gel-like structure rather than a

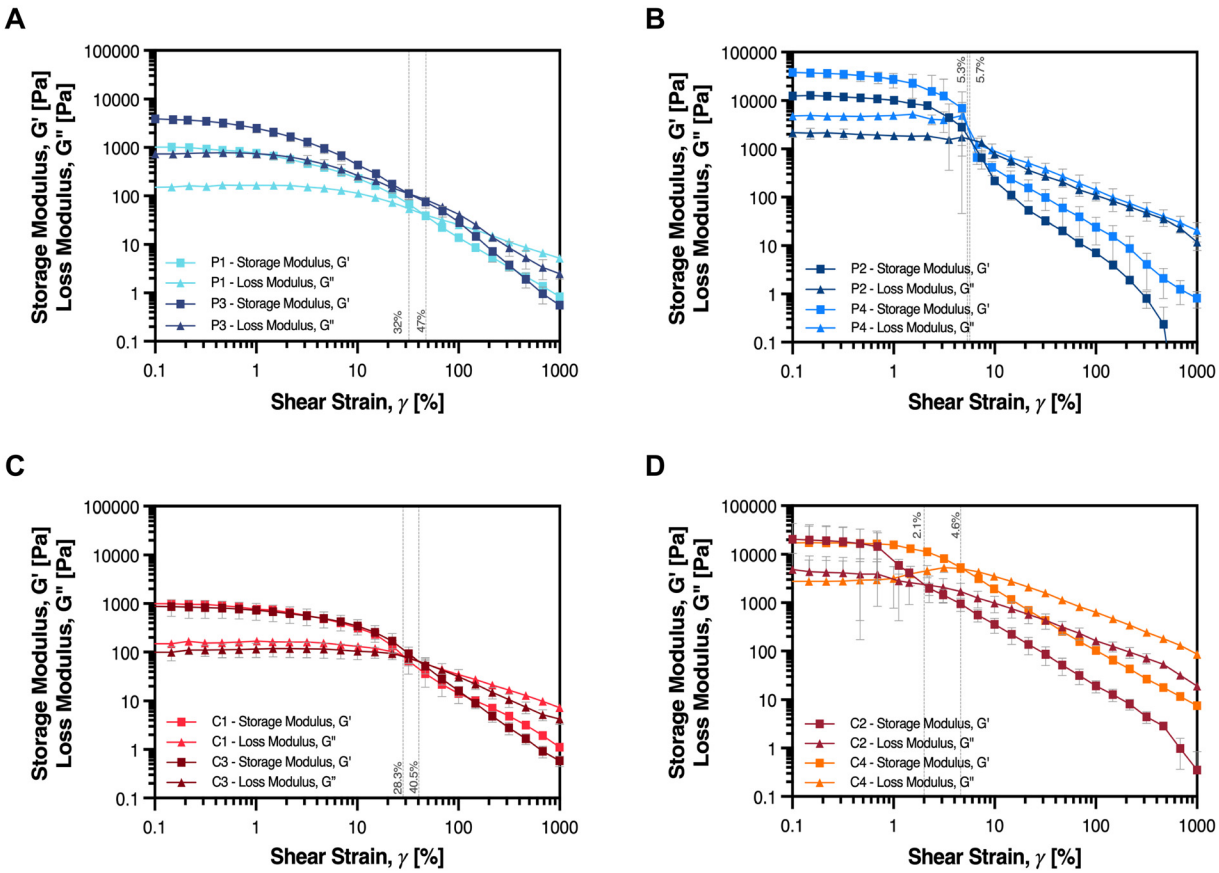

Fig. 5 Rheological measurements of all the prepared hydrogels. Amplitude sweep tests showing breaking points (ε) of (A) P1 and P3 hydrogels, (B) P2 and P4 hydrogels, (C) C1 and C3 hydrogels, and (D) C2 and C4 hydrogels.

creamy one. This feature does not represent an intrinsic limitation; rather, it reflects the reduced ability of the gel to flow or spread under mechanical stress.

Overall, these results demonstrate that the rheological properties of nanocellulose-based hydrogels can be finely tuned through chemical modifications and crosslinking strategies, enabling the rational design of materials with mechanical characteristics tailored to specific biomedical applications.

From an application point of view, these rheological features are particularly advantageous for locoregional medical applications, such as hydrogel deposition following surgical resection of solid tumors, subcutaneous injections, and injectable scaffolds for tissue engineering. In such contexts, a stiffer and less deformable hydrogel is more likely to remain localized at the site of application, minimizing undesired diffusion into surrounding tissues and prolonging residence time. Therefore, despite their lower breaking strain, CNCs–COOH–CHO-based hydrogels represent a promising platform for post-surgical local delivery systems, where local retention and controlled spatial confinement are critical requirements.

The gels were thus tuned to exhibit a storage modulus (G') of ~10^2–10^3 Pa and a loss modulus (G'') of ~10^1–10^2 Pa, values representative of soft tissues, including brain,[19] subcutaneous tissue,[20] and other compliant biological environments.[21] The condition $G' > G''$ within the linear viscoelastic region ensured a stable solid-like behaviour. In addition, injectability was evaluated by viscosity measurements as a function of the shear rate, revealing pronounced shear-thinning behaviour (see SI Fig. S10A for an example of viscosity measurement on the C3 hydrogel). Under the high shear conditions experienced during syringe extrusion, viscosity decreased markedly, thus enabling minimally invasive delivery. Amplitude sweep tests repeated after the injectability (viscosity) test (Fig. S10B) confirmed that G' remained greater than G'' and comparable to pre-injection values, indicating the recovery of the gel's solid-like network following shear stress.

Finally, maintaining G' greater than G'' after extrusion indicates that the gel network recovers its solid-like character following the high shear experienced during injection, consistent with standard rheological characterization of injectable hydrogels.[22]

2.2.4. Scanning electron microscopy (SEM) characterization. SEM images demonstrated that all hydrogels presented a homogeneous and porous network, as shown in Fig. 6. Hence, all these structures turned out to be suitable for drug delivery systems in which a sustained and prolonged release of the drug is needed.

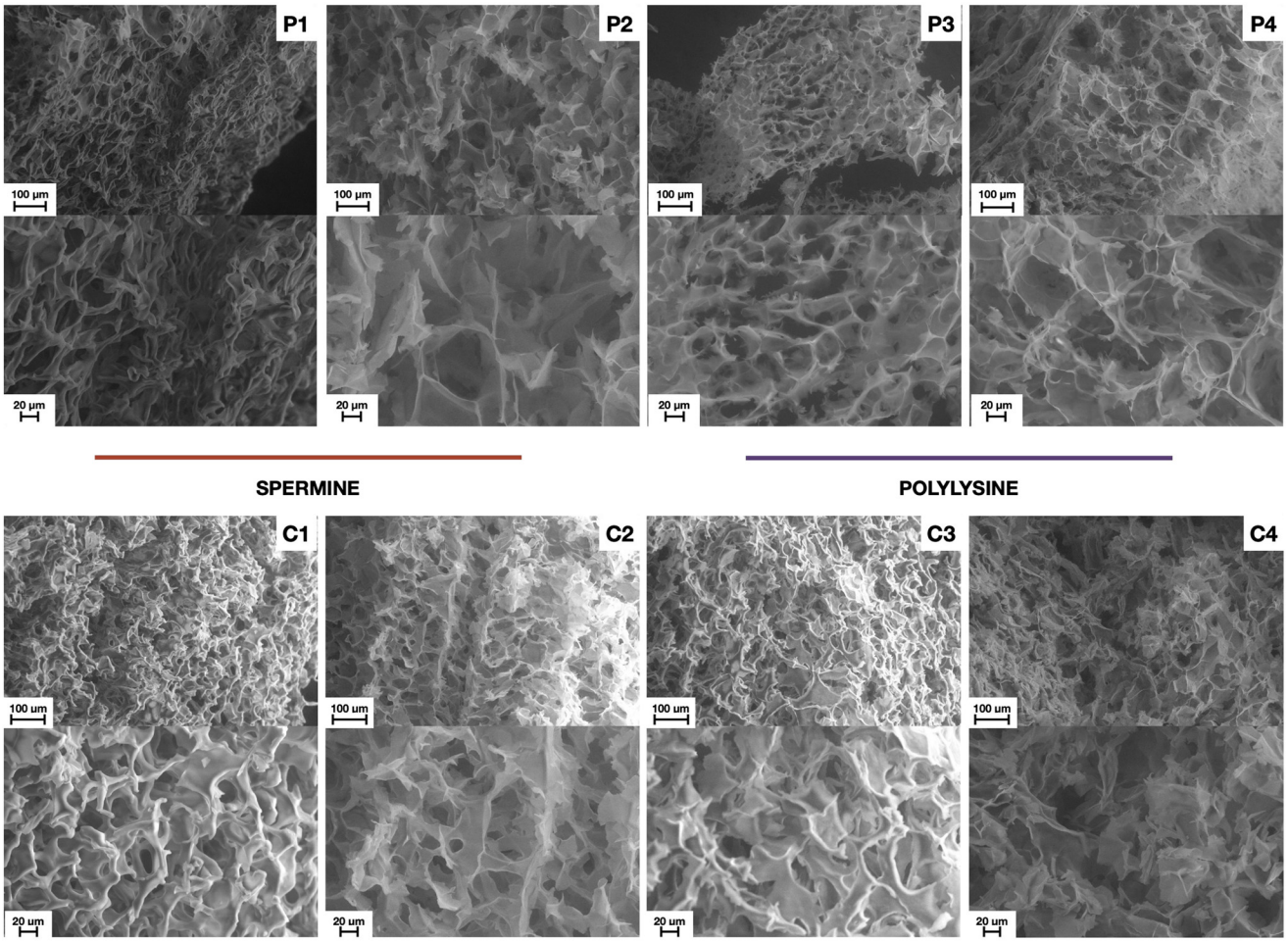

Fig. 6 SEM images of cross-sections of physical (P1–P4) and chemical (C1–C4) hydrogels.

A qualitative correlation between the rheological behavior and the microstructural features observed by SEM can be identified.

The highly porous architecture with interconnected pores exhibited by all synthesized hydrogels was consistent with their solid-like viscoelastic response and suitability for sustained drug delivery applications. However, notable differences in the pore morphology and size were observed depending on both the oxidation degree of nanocellulose and the crosslinking strategy employed. In particular, chemically crosslinked hydrogels exhibited smaller pore sizes, ranging approximately from 15 to 30 µm, whereas physically crosslinked hydrogels showed larger pores, typically between 30 and 45 µm. This reduction in pore size in chemically crosslinked systems can be attributed to the formation of permanent covalent bonds, which promote a denser and more compact polymer network. Such microstructural features are consistent with the rheological results obtained from amplitude sweep tests, where chemically crosslinked hydrogels exhibited higher resistance to deformation, a more stable linear viscoelastic region, and a lower tendency to structural rearrangement under increasing strain.

The cross-sectional area of all gels exhibited a channel-like structure in which the pores are more concentrated in the inner part of the gel and are interconnected. More specifically, the structures of C2, C4, P2 and P4 hydrogels, synthesized from bi-oxidized nanocellulose (CNCs–COOH–CHO), and different crosslinkers presented narrower folding and sheets, which could explain the rheological properties of these gels since their structure is tougher and stiffer compared to those of hydrogels made from mono-oxidized nanocellulose (CNCs–COOH), which are creamier.

Overall, although SEM provides static information on the dried-state microstructure, the observed trends in pore size and network compactness qualitatively support the rheological findings, suggesting that smaller pore dimensions and higher structural density correlate with increased stiffness and reduced deformability of the hydrogels. These results further highlight how chemical modification and a crosslinking approach can be effectively used to tune both the microstructural and mechanical properties of nanocellulose-based hydrogels.

2.2.5. Cytotoxicity analysis. Cytotoxicity tests (Fig. 7) have been performed on all hydrogels to check the toxicity of car-

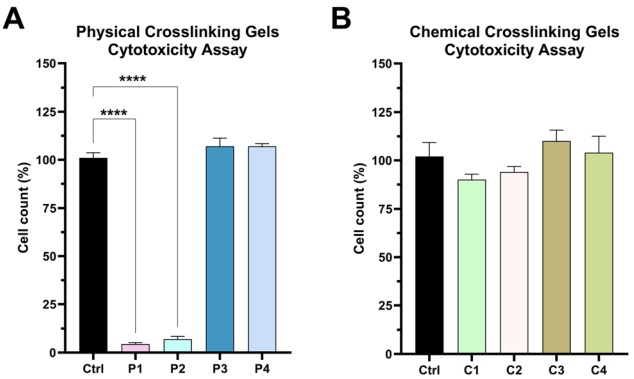

Fig. 7 *In vitro* biocompatibility of hydrogels tested on U87-MG glioblastoma cells. (A) Physical crosslinking gels series (P1–P4). P1 and P2 exhibited significant cytotoxicity (****$p < 0.0001$), while P3 and P4 did not exhibit any toxic effect. (B) Chemical crosslinking gels series (C1–C4), all of which showed no cytotoxic effect.

riers themselves before loading a drug. The analysis was performed by incubating the gels in cell culture medium for 16 hours at 37 °C; afterwards, the gel and culture media were centrifuged, and the supernatant was added to the cells. The U87-MG cell line was used for the test; it is derived from human glioblastoma and is one of the most commonly used cell models in neuro-oncology and neurobiology research.[23]

Cytotoxicity testing revealed a clear difference between the two-gel series (P and C). Specifically, among P series gels, P1 and P2 exhibited cytotoxic effects, while no such effect was observed in the C series. Cytotoxicity observed in P1 and P2 formulations could be caused by the unreacted free spermine. Notably, based on our results, among the C series gels, all are suitable candidates for future development, since the differences in viability are not statistically significant.

2.2.6. Doxorubicin release tests. Two hydrogels, C4 and P4, identified as two promising formulations from rheological property and cytotoxicity results, were loaded with an anticancer model drug (Fig. 8A), *i.e.* doxorubicin (DOXO), to test the drug release profile of this delivery system. In this study, doxorubicin was selected as a representative model drug to demonstrate the feasibility of sustained release from the proposed hydrogels. The modularity of the platform refers to the chemically programmable nature of the nanocellulose scaffold and crosslinking strategy, while extension to drugs with different physicochemical properties is envisioned as part of future investigations.

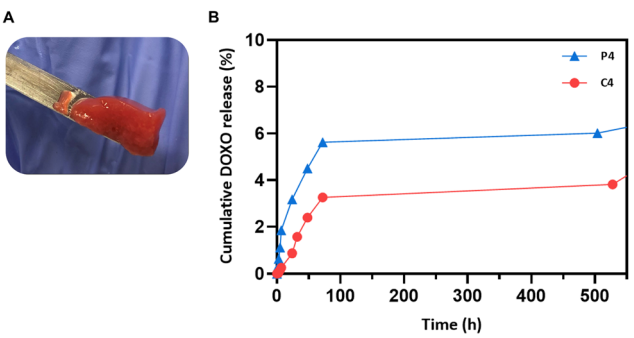

Fig. 8 (A) Hydrogel loaded with doxorubicin. (B) Drug release profiles of hydrogels C4 and P4.

An *in situ* encapsulation strategy was used, where the drug solution is incorporated into the polymer precursor solution before the gelation step. This method ensures homogeneous distribution and avoids diffusion limitations, leading to a high drug loading efficiency, potentially approaching 100%. The drug loaded in both gels was kept constant and equal to 55 μg mL^{-1}. Both hydrogels presented a slow and highly prolonged release, since the drug is still released after 21 days, as shown in Fig. 8B. C4 and P4 exhibited a sustained drug release profile in which a burst release of the drug is prevented; indeed, the total cumulative percentage of drug released at the end of the experiment from the physically crosslinked hydrogel P4 was 6.2%, whereas a release equal to 4.1% of the total drug loaded was observed in the drug release profile of the chemically crosslinked hydrogel C4. A release peak occurs at ~72 hours: delayed release peaks are commonly associated with progressive swelling and relaxation of the hydrogel network, leading to a rearrangement of the polymeric network and a gradual increase in mesh size which can be temporarily enlarged and facilitate drug diffusion.[24,25] Additionally, the drug released from physically crosslinked hydrogels is slightly higher than from chemically crosslinked systems, as the former have more dynamic and reversible crosslinks, promoting diffusion. In contrast, chemically crosslinked hydrogels form a more compact network, hindering drug release. These findings indicate that release kinetics are influenced by the temporal evolution of the hydrogel network, with the delayed peak at 72 hours reflecting controlled relaxation. This feature is crucial for minimizing the severe side effects of the drug released.

Using findings from the GDSC (Genomics of Drug Sensitivity in Cancer) Project[26] in which 32 glioblastoma cell lines were screened, a potential therapeutic efficacy was evaluated. According to these data, the minimum IC50 is 0.00723 μM, the maximum is 19.2 μM and the geometric mean is equal to 0.206 μM. We used this database to estimate a hypothetical effective dose within our controlled-release platform. Regarding the chemically crosslinked gel C4, the released drug concentration reached 0.0202 μM after 2 hours, and 3.80 μM after 21 days, whereas it reached 0.121 μM after 2 hours when released from the physically crosslinked gel P4, and 6.09 μM after 21 days. All these concentrations fall within the effective range reported by the GDSC Project, suggesting that the system could achieve therapeutically relevant concentrations for the majority of glioblastoma cell lines.

3. Experimental section

3.1. Materials

All chemicals were purchased from Merck KGaA (Darmstadt, Germany) and used as received. All aqueous solutions were

prepared with deionized water obtained using an ultrafiltration system (Milli-Q, Millipore, Burlington, MA, USA) with a measured resistivity above 18 MΩ cm^{-1}.

3.2. Synthesis of cellulose nanocrystals (CNCs)

CNCs were isolated and prepared by sulfuric acid hydrolysis. Whatman cellulose filter paper (14.8 g) was finely cut into small pieces and placed in a round-bottomed flask. DI water (100 mL) was cooled in an ice bath, and then concentrated sulfuric acid (100 mL; 98 wt%) was added slowly to the DI water. The diluted sulfuric acid solution was then added slowly, with continuous mixing, to the cellulosic filter paper. The reaction mixture was heated to 50 °C for 1 hour with continuous stirring. Hydrolysis was stopped by the addition of 200 mL of ice-cold DI water. The acid in the resultant suspension was then removed by centrifugation (Sartorius Centrisart G-16) at 9000 rpm for 15 minutes. This was repeated three times. In between each cycle, the supernatant was removed, and fresh DI water was added. After the final cycle of centrifugation, the creamy sediment was transferred into SnakeSkin™ Dialysis Tubing (3.5 K MWCO, 22 mm) for purification by dialysis. Dialysis was performed against DI water until a constant neutral pH was reached. The DI water was replaced twice each day. Upon completion of dialysis, the CNCs isolated were stored in the fridge at 4 °C at a concentration of 15 mg mL^{-1} measured by gravimetric analysis.

3.3. TEMPO-oxidation of CNCs to produce CNCs–COOH

(2,2,6,6-Tetramethylpiperidin-1-yl)oxidanyl (TEMPO; 665.6 mg) and NaBr (6.4 g) were added to 690 mL of nanocellulose suspension under stirring (10.35 g; 15 mg mL^{-1}), followed by dropwise addition of NaOCl 14% Cl_2 (6.3 mL). The mixture was basified to pH 10 through the addition of NaOH (0.1 M) and left to react for 90 minutes at room temperature. To quench the reaction, MeOH (45.6 mL) was added, followed by HCl (0.1 M) to neutralize the solution. The mixture was centrifuged at 9000 rpm for 15 min, and the precipitate was re-suspended in the minimum amount of DI water. SnakeSkin™ Dialysis Tubing (3.5 K MWCO, 22 mm) was used to complete the purification by dialysis against water for 3 days. The product was stored at 4 °C.

3.4. $NaIO_4$ oxidation of CNCs–COOH to produce CNCs–COOH–CHO

In a round-bottomed flask covered in aluminum foil, $NaIO_4$ (4.94 g) was added to CNCs or CNCs–COOH (600 mL; 16 mg mL^{-1}). The reaction mixture was left to stir in darkness at room temperature for 3 days, followed by purification by dialysis against water for 7 days. A silver nitrate ($AgNO_3$) test was carried out to ensure that the purification was finished. The products 3 and 4 were stored at 4 °C.

3.5. CNCs–COOH/CNCs–COOH–CHO hydrogel physically crosslinked with spermine and ε-poly-L-lysine

CNCs–COOH/CNCs–COOH–CHO (40–45 mg mL^{-1}; 1.8 mL) was mixed for 10 minutes in an ultrasonic bath with spermine (250 mg mL^{-1}; 200 μL) and calcium chloride (10 mg mL^{-1}; 60 μL). Then, it was left to jellify overnight at 35 °C.

CNCs–COOH/CNCs–COOH–CHO (50 mg mL^{-1}; 1.8 mL) was mixed for 1 minute with ε-PLL (40 mg mL^{-1}; 60 μL) using a vortex. Then, it was left to jellify overnight at room temperature. The hydrogel's appearance was creamy when starting from CNCs–COOH and more jelly-like for CNCs–COOH–CHO gels. All gels passed the tilt test (see SI, Fig. S11).

3.6. CNCs–COOH/CNCs–COOH–CHO hydrogel chemically crosslinked with spermine and ε-poly-L-lysine

CNCs–COOH/CNCs–COOH–CHO (40–45 mg mL^{-1}; 1.8 mL) was mixed for 10 minutes with 1-ethyl-3-(3-dimethylaminopropyl)carbodiimide (EDC) (39 mg) and *N*-hydroxysuccinimide (NHS) (23 mg); then, respectively, spermine (20 mg mL^{-1}; 200 μL) or ε-poly-L-lysine (40 mg mL^{-1}; 80 μL), and calcium chloride (3 mg mL^{-1}; 60 μL) were added. The reagents were mixed with a glass rod and then left to jellify overnight at room temperature with spermine or +4 °C with ε-PLL (see SI Fig. S11). A small amount of NaOH (0.025 M, 200 μL) was added the day after to neutralise the pH, if necessary, and to remove the free reagents, a wash with 1 mL of ID water was performed. Gels formulated starting from CNCs–COOH appeared creamy, whereas gels prepared with CNCs–COOH–CHO were stiffer and jelly-like. All hydrogels passed the tilt test (see SI Fig. S12 for the mechanism of the reaction).

To determine the optimum formulation for both chemical and physical hydrogels, functionalised nanocellulose and di-/polyamine compositions of gels were varied and a broad range of concentrations were examined:

- CNCs–COOH concentrations tested: 1, 1.5, 2, 2.5, 3, 3.5, 4.5, 5, 5.5, and 6% w/w. The suspension was gradually concentrated by rotary evaporation.

CNCs–COOH–CHO concentrations evaluated: 1, 2, 3, 4, 4.5 and 5% w/w. In the case of CNC–COOH–CHO 5.5% w/w, the gels turned out to be too solid, so a more concentrated suspension was not taken into account.

- Spermine concentrations screened: 0.1, 0.2, 0.4, 1, 1.8 and 2.5% w/w of the total gel. Assuming that the 2 ml gel had a mass of 2 g, 0.1% w/w corresponded to 2 mg of spermine. Therefore, the masses tested were from 2 to 50 mg.
- ε-poly-L-lysine (ε-PLL) concentrations tested: 0.05, 0.08, 0.1, 0.2, 0.4 and 0.8% w/w of the total gel. At an ε-PLL concentration of 1% w/w, a significant shrinkage was observed.

For additional details, see the SI, Tables S8 and S9.

3.7. Materials characterization

Centrifugation was performed on a Sartorius G-16 centrifuge equipped with a YCSR-A0B fixed-angle rotor. Attenuated total reflectance Fourier transform infrared (ATR-FTIR) measurements were performed using the Spotlight 200i FT-IR microscopy system with Spectrum 3 (PerkinElmer), equipped with a thermal source (Globar) and a deuterated triglycine sulfate (DTGS) detector. A single-reflection ATR accessory from PIKE Technologies with a diamond Internal Reflection

Element (IRE) was used. Spectra were acquired with a spectral resolution of 4 cm^{-1} over the range of 600–4000 cm^{-1}, averaging 64 scans to improve the signal-to-noise ratio and enhance spectral quality. Atmospheric contributions were corrected, and baseline correction and normalization were performed using Origin 2025b software.

SEM images were acquired with a field emission gun scanning transmission electron microscope ZEISS LEO Gemini 1530 (FEG-STEM) (Jena, Germany). ζ-Potential measurements were performed using a Malvern (Malvern, UK) Zetasizer Nano-S with a 532 nm laser beam in DTS1070 clear disposable zeta cells at 25 °C.

Rheological characterization was performed using an MCR 102 Anton Paar rheometer equipped with a parallel plate geometry with DPP25 as the upper plate. The amplitude sweep test was used to assess the viscoelastic properties of the gels under increasing strain. The test was performed using a plate-plate geometry on the Anton Paar rheometer, with an upper component having a 25 mm diameter and a 0.4 mm gap between the bottom plate on which the sample is placed and the upper plate. A constant angular frequency of 1 Hz was applied while gradually increasing the strain from 0.1% to 1000%. This method was used to identify the Linear Viscoelastic Region (LVR), the range within which the gel's structure remains stable and consistent.

The concentration of carboxylic acid groups present in the CNCs–COOH sample was determined with a conductometric titration. In particular, an Amel 2131 conductivity meter connected to an Amel 192/K1 probe was employed, and the cell constant was determined with a standard 0.1 M KCl solution at 22 °C. The pH of the acidified sample was measured with an XS sensor standard 0–14 pH glass electrode connected to an XS Instruments 8|80 pH meter. The titration was performed with a Witeg burette (25.00 ± 0.03 mL at 20 °C). The conductometric titration was carried out by the gradual addition of 0.100 M NaOH adapting a method reported by Bauer, Henry H. *et al.*[27]

Regarding drug release tests, hydrogels loaded with the drug were placed into an Eppendorf tube presenting a dialysis membrane (D-Tube Dialyzer Midi), immersed in PBS buffer (Fig. S13) and incubated at 37 °C. At regular time intervals (every 1 h for the first 8 hours and then at 12, 24, 48 hours and so on), 1 mL of the buffer was withdrawn and replaced with freshly preheated phosphate buffer solution. The calibration curve was created using 5 standard solutions with known concentrations of the drug (see SI, Fig. S14) at pH 7.4 and all drug release content was analysed through HPLC with UV detection using 1260 Infinity II Agilent LC/MSD equipped with a 5 μm C18 column Poroshell 120 EC-C18 (4.6 × 150 mm).

3.8. Cytotoxicity assay

The glioblastoma U87-MG cell line was purchased by PerkinElmer. U87-MG cells were cultured in Eagle's Minimum Essential Medium (EMEM; ATCC, USA), supplemented with 10% fetal bovine serum (Gibco, USA), 2 mM L-glutamine, and 100 units per mL penicillin–streptomycin (EuroClone) and maintained at 37 °C under an atmosphere of 5% CO_2/air. To test the effect of the gels on U87-MG cells, they were seeded at a density of 7 × 104 cells per well in 12-well plates, in triplicate. Gels were incubated in cell culture medium for 16 hours at 37 °C. 24 hours after seeding, the gel and culture media were centrifuged, and the supernatant was added to the cells. After 24 h of incubation, cells were washed in PBS and harvested. The cell number of each sample was determined with a Z2 Coulter Counter (Beckman Coulter), in triplicate. Data about cell viability were plotted in GraphPad Prism 8.0 software (GraphPad Software). Statistical analysis was performed using an unpaired *t* test with Welch's correction.

4. Conclusion

In this work, we successfully introduced a dual and orthogonal functionalization of cellulose nanocrystals by combining TEMPO- and periodate-mediated oxidation, yielding stable carboxy and dialdehyde groups on the same scaffold. This unprecedented modification enabled the design of modular hydrogel systems through both physical and chemical crosslinking with biocompatible diamines. The resulting hydrogels showed tunable mechanical properties, homogeneous porosity, and excellent *in vitro* biocompatibility. Importantly, the selected formulations achieved sustained, burst-free release of doxorubicin for over three weeks, overcoming a key limitation of current nanocellulose-based drug delivery systems. These results underscore the potential of bifunctional CNCs as versatile building blocks for advanced biomaterials, enabling customizable injectable hydrogels for localized cancer therapy and related applications.

Author contributions

EB, CS, MZ, LS, and GI: data curation, formal analysis, investigation, methodology, and writing – original draft. MCF, MC, TS, LS, and EV: project administration, supervision, validation, and writing – review & editing. EL: conceptualization, project administration, resources, supervision, and writing – review & editing.

Conflicts of interest

The authors declare that they have no conflicts of interest.

Data availability

All data supporting the findings of this study are available within the paper and its supplementary information (SI). Supplementary information is available. See DOI: https://doi.org/10.1039/d5bm01841b.

Acknowledgements

This research was funded in part under the National Recovery and Resilience Plan (NRRP), Mission 6, Component 2, Investment 2.1, published on 24.04.2023 by the Italian Ministry of Health (PNRR-TR1-2023-12377370), funded by the European Union – NextGenerationEU – Project Title: Locoregional administration of therapeutic hydrogels to overcome the blood–brain barrier and prevent glioblastoma recurrences, CUP F13C23003200006 (Unit 1), CUP B53C23008320006 (Unit 2), CUP J33C23004200006 (Unit 3), and CUP B63C23001870006 (Unit 4). This research was funded in part by Regione Toscana (Italy) to MC, in the context of the ERA-NET TRANSCAN-3 initiative (Project: SeqPerGlio; ref. TRANSCAN2024-2930-062).

References

1 B. Thomas, M. C. Raj, K. B. Athira, M. H. Rubiyah, J. Joy, A. Moores, G. L. Drisko and C. Sanchez, *Chem. Rev.*, 2018, **118**, 11575–11625.
2 A. Isogai, T. Saito and H. Fukuzumi, *Nanoscale*, 2011, **3**, 71–85.
3 A. Errokh, A. Magnin, J.-L. Putaux and S. Boufi, *Cellulose*, 2018, **25**, 3899–3911.
4 D. J. Mendoza, C. Browne, V. S. Raghuwanshi, G. P. Simon and G. Garnier, *Carbohydr. Polym.*, 2019, **226**, 115292.
5 G. Patterson and Y.-L. Hsieh, *Nanoscale Adv.*, 2020, **2**, 5623–5634.
6 A. K. Tamo, *J. Mater. Chem. B*, 2024, **12**, 7692–7759.
7 S. Correa, A. K. Grosskopf, H. Lopez Hernandez, D. Chan, A. C. Yu, L. M. Stapleton and E. A. Appel, *Chem. Rev.*, 2021, **121**, 11385–11457.
8 S. Liu, S. A. Qamar, M. Qamar, K. Basharat and M. Bilal, *Int. J. Biol. Macromol.*, 2021, **181**, 275–290.
9 R. Nicu, F. Ciolacu and D. E. Ciolacu, *Pharmaceutics*, 2021, **13**, 1125.
10 M. Maturi, C. Spanu, A. Baschieri, M. Comes Franchini, E. Locatelli and L. Sambri, *Biomolecules*, 2022, **12**, 1165.
11 C. Lin, T. Zeng, Q. Wang, L. Huang, Y. Ni, F. Huang, X. Ma and S. Cao, *BioResources*, 2018, **13**, 5965–5975.
12 L. Chen, W. Cao, P. J. Quinlan, R. M. Berry and K. C. Tam, *ACS Sustainable Chem. Eng.*, 2015, **3**, 978–985.
13 Q. Li, P. Sritharathikhun and S. Motomizu, *Anal. Sci.*, 2007, **23**, 413–417.
14 P. Nonsuwan, A. Matsugami, F. Hayashi, S.-H. Hyon and K. Matsumura, *Carbohydr. Polym.*, 2019, **204**, 131–141.
15 A. Bertoluzza, C. Fagnano, P. Finelli, M. A. Morelli, R. Simoni and R. Tosi, *J. Raman Spectrosc.*, 1983, **14**, 386–394.
16 J.-N. Liu, S.-L. Chang, P.-W. Xu, M.-H. Tan, B. Zhao, X.-D. Wang and Q.-S. Zhao, *J. Agric. Food Chem.*, 2020, **68**, 1101–1109.
17 M. Nochi, Y. Ozaki and H. Sato, *Spectrochim. Acta, Part A*, 2021, **260**, 119900.
18 A. Iwasaki, A. Fujii, T. Watanabe, T. Ebata and N. Mikami, *J. Phys. Chem.*, 1996, **100**, 16053–16057.
19 C. C. Parkins, J. H. McAbee, L. Ruff, A. Wendler, R. Mair, R. J. Gilbertson, C. Watts and O. A. Scherman, *Biomaterials*, 2021, **276**, 120919.
20 C. F. Guimarães, L. Gasperini, A. P. Marques and R. L. Reis, *Nat. Rev. Mater.*, 2020, **5**, 351–370.
21 A. Hatt, R. Lloyd, B. Bolsterlee and L. E. Bilston, *J. Mech. Behav. Biomed. Mater.*, 2023, **143**, 105924.
22 C. Yan, A. Altunbas, T. Yucel, R. P. Nagarkar, J. P. Schneider and D. J. Pochan, *Soft Matter*, 2010, **6**, 5143.
23 L. Gherardini, V. Vetri Buratti, M. Maturi, G. Inzalaco, E. Locatelli, L. Sambri, S. Gargiulo, V. Barone, D. Bonente, E. Bertelli, S. Tortorella, L. Franci, A. Fioravanti, M. Comes Franchini and M. Chiariello, *Sci. Rep.*, 2023, **13**, 4630.
24 N. Peppas, *Eur. J. Pharm. Biopharm.*, 2000, **50**, 27–46.
25 J. Siepmann and F. Siepmann, *J. Controlled Release*, 2012, **161**, 351–362.
26 Genomics of Drug Sensitivity in Cancer. URL: https://www.cancerrxgene.org/compound/Doxorubicin/133/overview/ic50?tissue=GBM&screening_set=GDSC1.
27 H. H. Bauer, D. C. Gary and J. E. O'Reilly, *Analisi strumentale*, 1985.